

# Effect of nano-Nb<sub>2</sub>O<sub>5</sub> on the microstructure and mechanical properties of AZ31 alloy matrix nanocomposites

Song-Jeng Huang<sup>a</sup>, Sathiyalingam Kannaiyan\* and Murugan Subramani<sup>b</sup>

Department of Mechanical Engineering, National Taiwan University of Science and Technology, Taipei, 10607, Taiwan, (ROC)

(Received October 20, 2021, Revised August 15, 2022, Accepted August 27, 2022)

**Abstract.** In this study, the gravitating mechanical stir casting method was used to fabricating the Nb<sub>2</sub>O<sub>5</sub>/AZ31 magnesium matrix nanocomposites. Niobium pentoxide (Nb<sub>2</sub>O<sub>5</sub>) used as reinforcement with two different weight percentages (3 wt % and 6 wt %). The influence of Nb<sub>2</sub>O<sub>5</sub> on microstructure and mechanical properties has been investigated. The microstructure analysis showed that the composites are mainly composed of the primary  $\alpha$ -magnesium phase and phase  $\beta$ -Mg<sub>17</sub>Al<sub>12</sub> secondary phase. The secondary phase was dispersed evenly along the grain boundary of the Mg phase. The Nb<sub>2</sub>O<sub>5</sub>/AZ31 nanocomposites revealed that the grain size and its lamellar shape ( $\beta$ -Mg<sub>17</sub>Al<sub>12</sub>) were gradually refined. Different strengthening mechanisms were assessed in terms of their contributions. Results showed that composite material properties of hardness, yield strength, and fracture study were directly related to Nb<sub>2</sub>O<sub>5</sub> as a reinforcement. The maximum values of the mechanical properties were achieved with the addition of 3 wt% Nb<sub>2</sub>O<sub>5</sub> on the AZ31 alloy.

**Keywords:** casting; mechanical properties; mechanical testing; metal-matrix composites (MMCs); microstructural analysis; nanocomposites,

## 1. Introduction

Research has increased substantially in recent years on product development to improve the performance of vehicles in the automotive and aerospace industries. Investigators have encountered many challenges in the enhancement of the ration between high strength and light weight (Ali Ghorbanpour Arani 2021). The best cost-effective solution is using alternative materials. Research on magnesium as a substitute for cast iron, aluminum and polymers has rapidly progressed (Chen *et al.* 2015, Abbas and Huang 2020a, Vini and Daneshmand 2020).

Magnesium-based alloys have attracted considerable attention as lightweight materials because of their low densities (approximately two-thirds of the density of aluminum), high specific strength, excellent castability, machinability and great damping capability. However, the application of magnesium alloys is limited because of its low strength, ductility and toughness at room temperature (Dey and Pandey 2015, Shen *et al.* 2020). These limitations have impeded their use as structural materials in critical engineering applications. Many researchers have attempted to improve the strength of magnesium materials by including carbides, oxide particles, carbonaceous, alloys and deformation procedures (Sameer Kumar *et al.* 2017, Dinaharan *et al.* 2020).

Metal matrix composites (MMCs) have attracted attention because combining a matrix and reinforcing material result

in a composite with excellent mechanical capabilities. Metal matrix composites are apparently isotropic materials, and production methods are similar to the production of monolithic materials (Khandelwal *et al.* 2017, Zhou *et al.* 2020). Some researchers used a stir casting process to create an AZ31 matrix composite from graphene nanoplatelets. The microhardness and tensile strength of the composites were higher than those of the magnesium alloy AZ31 (Rashad *et al.* 2015). Banerjee *et al.* (2019) used an ultrasonic vibration-assisted stir casting process to create AZ31-WC composites with WC concentrations ranging from 0.5 wt percent to 2 wt percent. The inclusion of WC nano-particles greatly improved the wear, friction and hardness of the AZ31 alloy. The behavior of an AZ31B/nano Al<sub>2</sub>O<sub>3</sub> composite prepared using the disintegrated melt deposition process. Under normal loads, the composite wear rate steadily decreased with sliding speed. The wettability of fly ash particles is sufficient for stir casting reinforcement into AZ31 (Dinaharan *et al.* 2019). Niobium pentoxide (Nb<sub>2</sub>O<sub>5</sub>) is insoluble nature in water and excellent durability. Nb<sub>2</sub>O<sub>5</sub> is widely used in ceramic structures from simple clay bowls to novel electronics components, light weight aerospace structural components and fuel cell applications (Zhu *et al.* 2011). The fineness and compactness of the microstructures of the composites increase with Nb<sub>2</sub>O<sub>5</sub> concentration and thereby contribute to increases in density, hardness, wear resistance and flexural strength. The properties of Nb<sub>2</sub>O<sub>5</sub> include excellent thermal, chemical, and thermodynamic stability, high reflective indices, excellent mechanical properties, and excellent fracture toughness. The superior catalytic property of Nb<sub>2</sub>O<sub>5</sub> enabled hydrogen absorption and desorption, along with biomedical and sensors applications. Nb<sub>2</sub>O<sub>5</sub> has not yet been fully explored in terms of its potential benefits and applications.

\*Corresponding author, Ph.D. Student,

E-mail: sathiaerospace@gmail.com

<sup>a</sup>Professor

<sup>b</sup>Ph.D.

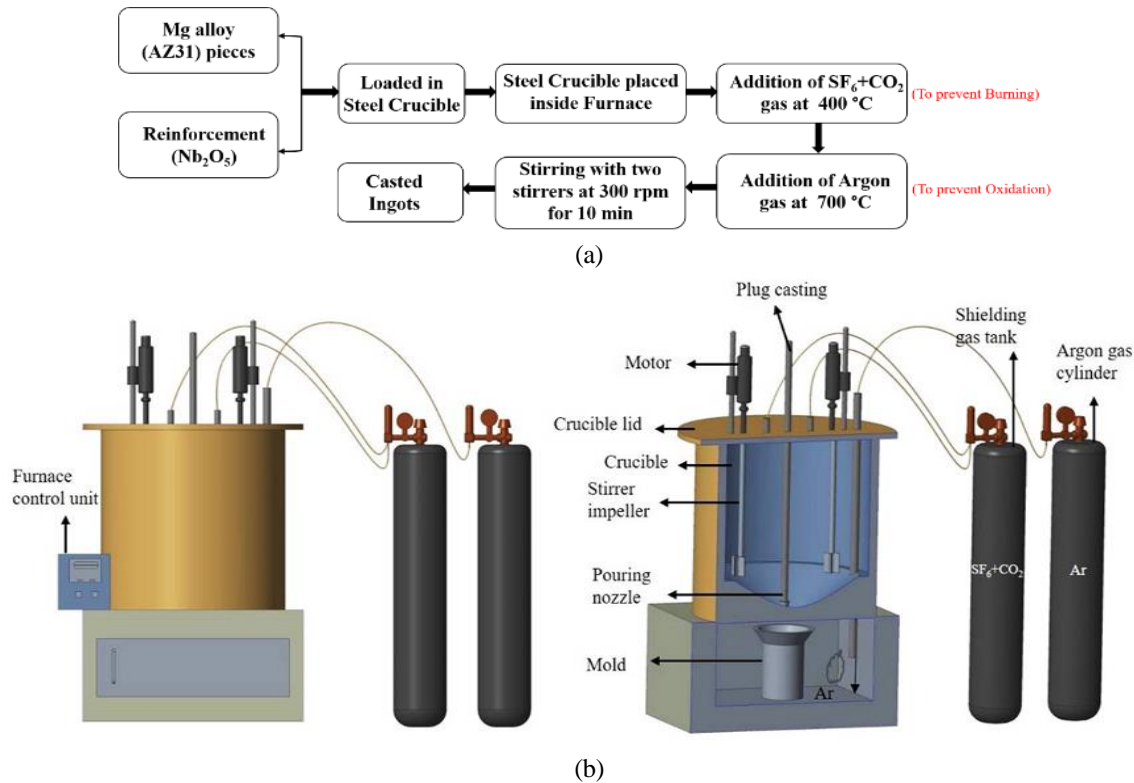


Fig. 1(a) Stir casting process steps; (b) Schematic diagram of the stir casting setup and sectional view

Due to their low wear resistance, low hardness, and low malleability, the Mg–Zn alloys have some disadvantages which limit their use. Nb<sub>2</sub>O<sub>5</sub> as reinforcement help to overcome limitation in magnesium matrix composite (Safavi *et al.* 2022). Furthermore, fine microstructure and homogenous reinforcement distribution result from the casting of composites (Alaneme *et al.* 2020a, Silva *et al.* 2020). Nb<sub>2</sub>O<sub>5</sub> enhancement and increase in temperature increase the shrinking rate of composites. An optimum proportion of Nb<sub>2</sub>O<sub>5</sub> is conducive to grain growth and densification. At increased Nb<sub>2</sub>O<sub>5</sub> concentration, elastic strain, yield pressure, wear characteristics and impact loading resistance improved (Alaneme *et al.* 2020b).

Fabrication methods have a significant impact on the mechanical properties of magnesium composites. The amount of defects incorporated during the fabrication process has a substantial impact on the overall structural performance of MMCs (Huang and Ali 2018). Stir casting, spray deposition, powder metallurgy, squeeze casting, physical vapor deposition and electroplating are used in preparing MMCs (Hassan and Gupta 2006, Borodianskiy and Zinigrad 2015, Selivorstov *et al.* 2017, Zhao *et al.* 2017). Stir casting is widely preferred over other methods because of its simple procedure and cost effectiveness when applied to the fabrication of Mg-MMCs (Bains *et al.* 2016, Idrisi and Mourad 2019). There are several advantages to the stir casting process, including the ability to produce complex shaped ingots at low costs, machinability improvements and improved mechanical properties of composite materials, as well as a high rate of production. In general, appropriate volume fractions can add up to 30 percent volume fraction of a reinforcing material during the

Table 1 Magnesium AZ31 alloy composition (wt.%)

Mg	Al	Zn	Mn	Si	Cu	Ca	Fe	Ni
95.42	3.2	0.9	0.3	0.1	0.04	0.03	0.005	0.005

casting of metal matrix composites (Huang *et al.* 2021)

The objective of this research is to fabricate a novel magnesium nanocomposites and study the mechanical characteristics of AZ31 composites with varying Nb<sub>2</sub>O<sub>5</sub> weight fractions. The effects of nano size Nb<sub>2</sub>O<sub>5</sub> weight fraction on the microstructure and AZ31 alloy characteristics were examined. All characterization investigations have been performed to reveal the successful incorporation of Nb<sub>2</sub>O<sub>5</sub>/AZ31 nanocomposites and its properties. To the best of our knowledge, Nb<sub>2</sub>O<sub>5</sub>/AZ31 nanocomposites have not been fabricated with the stir casting technique and there is also a shortage of information about their mechanical characteristics.

## 2. Materials and methods

### 2.1 Composite preparation

AZ31 magnesium alloy was acquired from Kuangyue Co., Ltd., used as matrix material and 99.90% pure Nb<sub>2</sub>O<sub>5</sub> was acquired from Allychem Company Ltd. The chemical composition of the matrix metal shown in Table 1. The Nb<sub>2</sub>O<sub>5</sub> with a particle size of 100 nm was used as a reinforcement. The gravitating mechanical stir casting (GMSC) method was used in fabricating samples with three distinct types of composition as follows: AZ31-0 wt%-

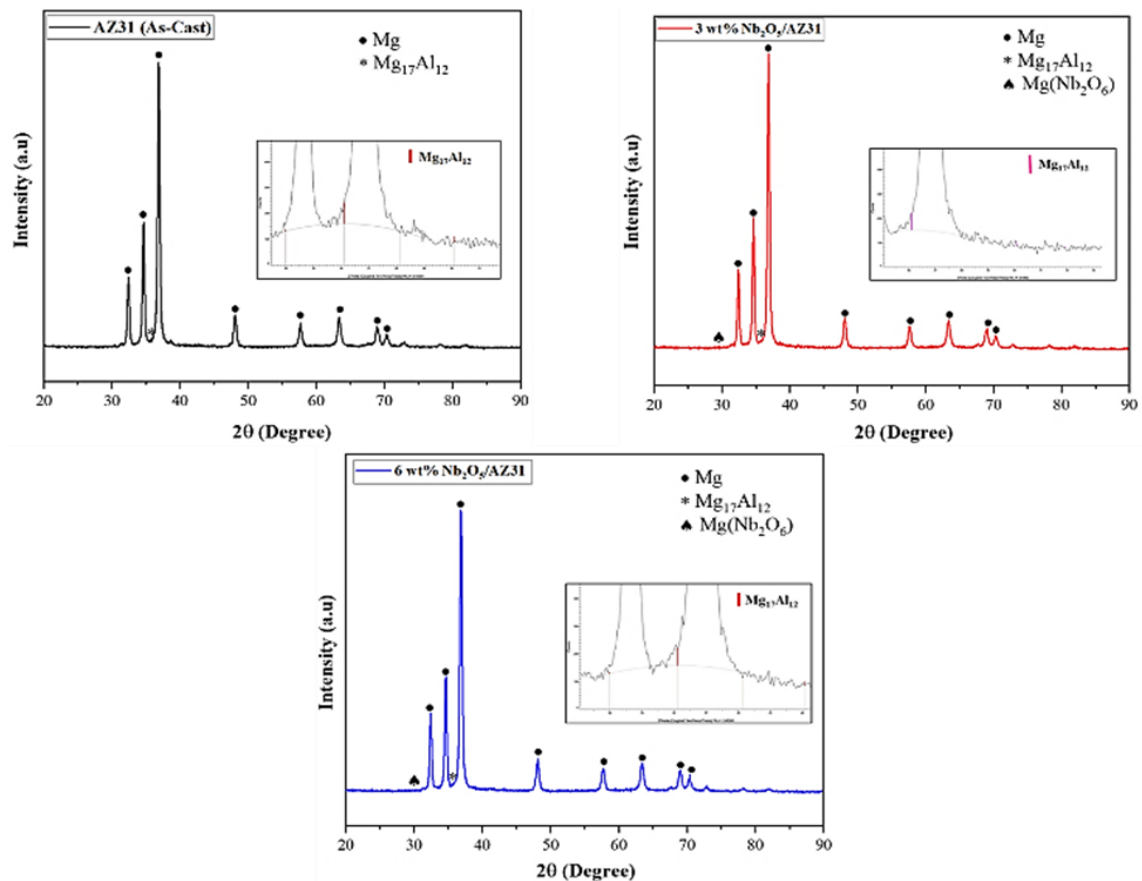


Fig. 2 XRD Pattern of the composites

Nb<sub>2</sub>O<sub>5</sub> (AZ31), AZ31-3wt% Nb<sub>2</sub>O<sub>5</sub> (3 wt% Nb<sub>2</sub>O<sub>5</sub>/AZ31) and AZ31-6wt%Nb<sub>2</sub>O<sub>5</sub> (6 wt% Nb<sub>2</sub>O<sub>5</sub>/AZ31). The AZ31 alloy bar was chopped down into pieces. The Mg alloy (AZ31) pieces along with reinforcement (Nb<sub>2</sub>O<sub>5</sub>) loaded in the steel crucible and kept inside electrical furnace. The combustion of magnesium alloy AZ31 was prevented by adding an SF<sub>6</sub>+CO<sub>2</sub> gas mixture at 400 °C during casting. Oxidation was prevented by adding argon (Ar) gas at 700 °C. The thermal stabilization time was maintained with 15 min for every 100 °C increase in temperature up to 700 °C during casting. In the casting process, mechanical stirring is used to distribute the reinforcing phases into the molten composite phase matrix. In this research, Nb<sub>2</sub>O<sub>5</sub>/AZ31 composite melt was stirred with two stirrers at 300 rpm for 10 min at 760 °C as shown in Fig. 1. This procedure ensured that Nb<sub>2</sub>O<sub>5</sub> was evenly distributed over the Mg alloy. The molten alloy was collected into a mold kept within the chamber used in making the ingots cast (Nb<sub>2</sub>O<sub>5</sub>/AZ31). By using the same approach and fabrication technique, three different types of cylindrical composite ingots (100mm height and 89mm diameter) were fabricated. The microstructural and mechanical investigation samples were prepared from the casted ingots. Mechanical grinding and polishing were performed for the preparation of specimens for microstructure examination in accordance with ASTM E3-11 standards. After the polishing process, the samples were etched in 100 ml of ethanol, 10 ml of DI water, 5 ml of acetic acid and 6 g of picric acid solution for 40 s before the testing of the microstructure. In order to determine the phase composition of

the composite sample, XRD was performed using the Bruker D2 phaser model and composite samples were subjected to Cu K  $\alpha$ -radiation at 45 kv and 0.8 mA. A scanning electron microscope (SEM) (model JSM-6390LV) equipped with an EDS was used to examining the microstructures of solid samples. The hardness was measured using an Akashi MVK-H1 micro Vickers hardness testing machine with diamond indenter. During the test, a load of 300gmf was applied and the holding time was 10 seconds. The results of five indentation measurements were used to determine the hardness of samples. Tensile samples were made in accordance with ASTM-E8-69 specifications, and tests were carried out on an MTS testing machine at a crosshead speed of 0.5 mm/min and loading capacity of 100 KN. Three specimens were tested for each composite and the final result was determined by using the average of the three specimens.

### 3. Result and discussion

#### 3.1 XRD analysis

The XRD examinations of as-cast Nb<sub>2</sub>O<sub>5</sub>/AZ31 nanocomposites samples phase composition were illustrated in Fig. 2. It can be depicted that the magnesium peaks are observed as a major phase and minor intensity peaks of secondary phase  $\beta$ -Mg<sub>17</sub>Al<sub>12</sub> (PDF 73-1148) in the Nb<sub>2</sub>O<sub>5</sub>/AZ31 nanocomposites, which can be attributed to the excellent crystallization phenomena achieved during the

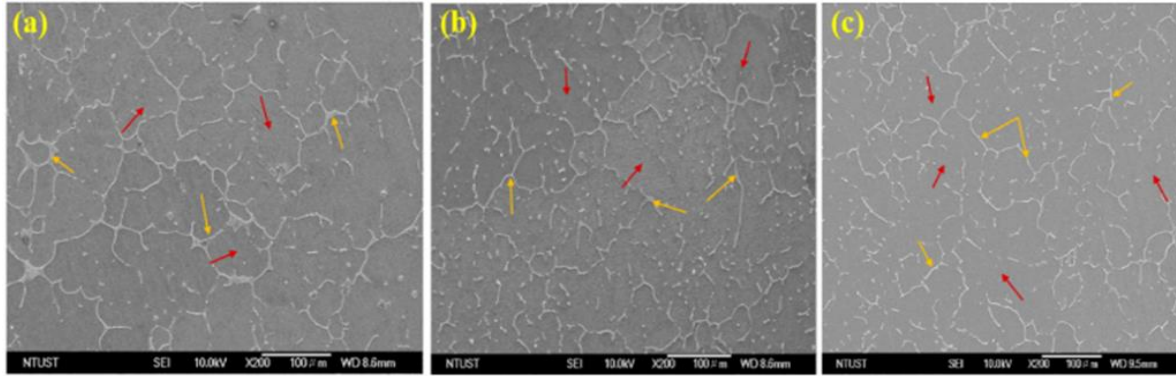


Fig. 3 SEM analysis images of (a) AZ31 (b) 3% Nb<sub>2</sub>O<sub>5</sub>/AZ31 (c) 6% Nb<sub>2</sub>O<sub>5</sub>/AZ31

Table 2 Quantitative XRD Analysis

Composition	Crystallites Size (D)(nm)	Dislocation Density $\delta \cdot 10^{-3} \text{ (nm}^{-2}\text{)}$	Grain Size ( $\mu\text{m}$ )
AZ31	16.63	3.77	34.67
3 wt% Nb <sub>2</sub> O <sub>5</sub> /AZ31	16.67	3.59	31.65
6 wt% Nb <sub>2</sub> O <sub>5</sub> /AZ31	16.30	3.91	32.11

fabrication process. The peak analysis reveals that the composites are containing the peak intensity of MgNb<sub>2</sub>O<sub>6</sub> (PDF 88-0708) phases. This indicates that the addition of Nb<sub>2</sub>O<sub>5</sub> to the alloy AZ31 resulted in the MgNb<sub>2</sub>O<sub>6</sub> phase. During the casting, the reaction between Mg (in AZ31) and Nb<sub>2</sub>O<sub>5</sub> forms MgO through oxidation. At 600 °C, MgO reacts with Nb<sub>2</sub>O<sub>5</sub> to form MgNb<sub>2</sub>O<sub>6</sub> based on the following reaction (Rahman 2019)



The textural difference may be calculated using the XRD peaks intensities at  $2\theta$  values of 32°, 34° and 36°, which correspond to the prismatic {10-10}, basal {0002} and pyramidal {10-11} planes of Mg crystals. The inclusion of Nb<sub>2</sub>O<sub>5</sub> in the AZ31 alloy thereby initiates the basal planes, and basal plane intensity is greater in Nb<sub>2</sub>O<sub>5</sub>/AZ31 nanocomposite than in the AZ31 alloy composite samples. The intensity changes of the basal plane can be suggesting that the existence of the Nb<sub>2</sub>O<sub>5</sub>.

Based on the results in table, it appears that the presence of Nb<sub>2</sub>O<sub>5</sub> in the composite may influence the recrystallization process, leading to smaller crystallite size. The Scherrer formula results in a smaller crystallite size than the actual grain size of the fabricated composites. In addition to the fact that the size of the crystallites is finite, there are also lattice imperfections and dislocation that can contribute to the peak broadening and grain size. The inhibiting effects of the reinforcement and the greater thermal stress produced during the cooling process caused increase in dislocations density of Nb<sub>2</sub>O<sub>5</sub>/A31 composites. The Grain size and residual stress are inversely related to dislocation density. A higher dislocation rate promotes grain growth, which accelerates precipitation kinetics. The combined interaction of dislocation density and grains size refinement enhancement of the Nb<sub>2</sub>O<sub>5</sub>/A31 composites (Abbas and Huang 2021).

### 3.2 Microstructural characteristics

The SEM and EDS (Figs. 3-4) images show that  $\alpha$ -Mg (red arrow) grains are surrounded by the secondary intermetallic phase  $\beta$ -Mg<sub>17</sub>Al<sub>12</sub> (yellow arrow) grains at the grain boundaries. The grain refinement in Mg-Al systems (Al concentration more than 1 wt%.) is mostly attributable to the superheating process. In the current investigation, the composites were fabricated at a superheated temperature of 750 °C and facilitates grain refinement in Nb<sub>2</sub>O<sub>5</sub>/AZ31 composite. The addition of Nb<sub>2</sub>O<sub>5</sub> to AZ31 alloy improves its resistance to coarsening and results in a smaller grain size. In accordance with coarsening models, grain size is directly related to surface energy, therefore a decrease in surface energy at a given temperature result in finer grains. The uniform temperature in the mold, nucleation and grain growth took place evenly. According to the free growth model, it has been found that nucleation growth can begin freely at different temperatures depending on the type of a matrix (da Silva *et al.* 2017). As a result, grains grow more rapidly as the temperature decreases. Microstructure refinement is also dependent upon a mismatch in coefficients of thermal expansion. Adding Nb<sub>2</sub>O<sub>5</sub> caused the thermal expansion mismatch, causing the grain boundaries to break down and the grains to become smaller. A reduction in the grain size was achieved with the nanoparticles, which resulted in an improvement in the microstructure of the composite (Borodianskiy and Zinigrad 2015). As a result, the density of the grain increases, and grain refinement provides greater strength to casted Nb<sub>2</sub>O<sub>5</sub>/AZ31 composites. From the EDS elemental mapping analysis revealed that the uniform distribution of nano Nb<sub>2</sub>O<sub>5</sub> particulates is observed in the composites. The uniformly distributed Nb<sub>2</sub>O<sub>5</sub> in molten AZ31 acts as a heterogeneous nucleus substrate, stimulating nucleation and limiting grain growth during solidification. The reason for the homogeneous distribution was the stable dispersion of nano Nb<sub>2</sub>O<sub>5</sub> particulates in the AZ31 magnesium alloy matrix during stirring. Pressure does not have a great impact on wetting behavior (Malaki *et al.* 2021). No apparent voids were observed at the interface between the Nb<sub>2</sub>O<sub>5</sub> and magnesium matrix, which indicating that the matrix and reinforcements were bonded well. As the Mg<sub>17</sub>Al<sub>12</sub> phases had adverse effects on mechanical properties, Nb<sub>2</sub>O<sub>5</sub> was added for the dissolution of precipitates and gradual

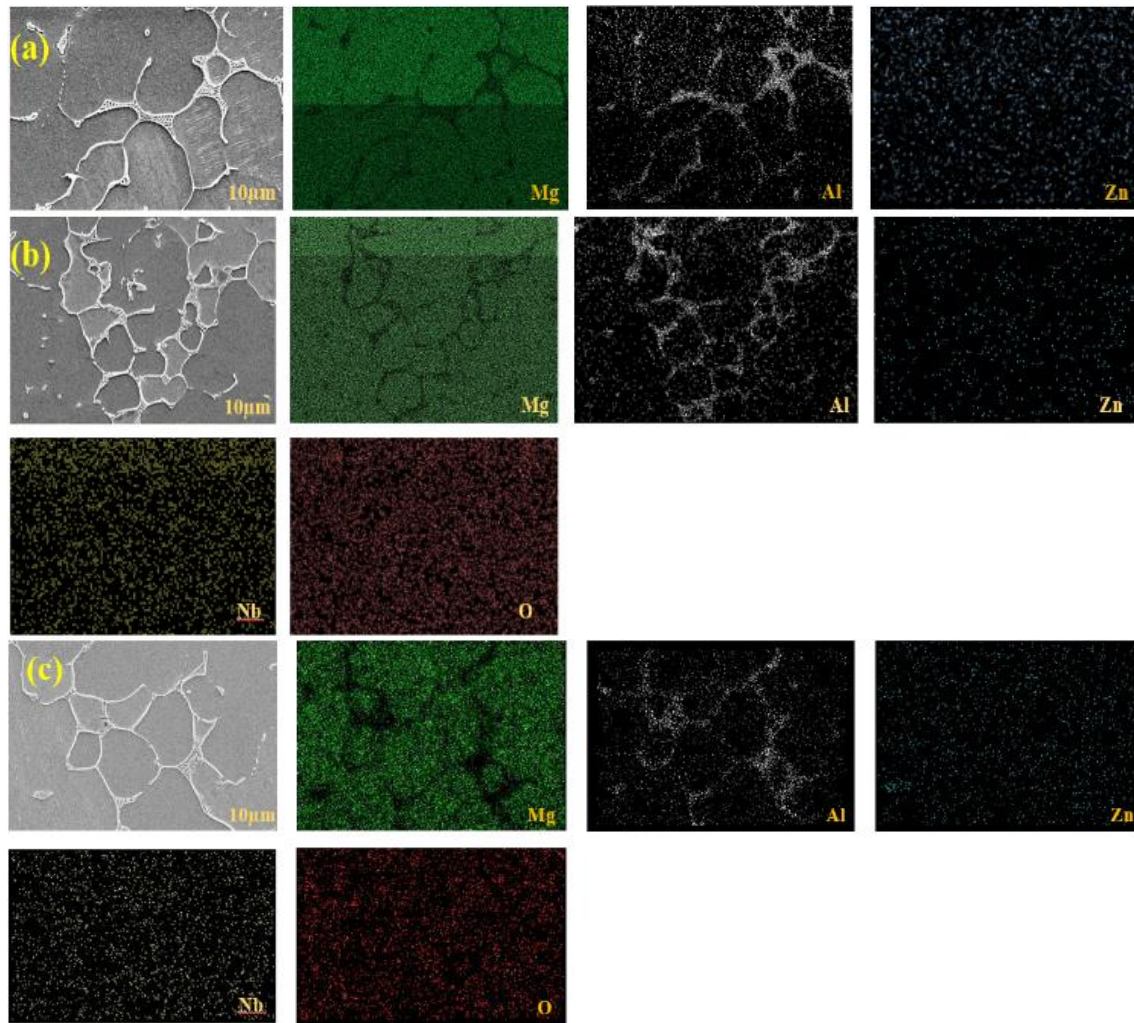


Fig. 4 EDS mapping images of (a) AZ31 (b) 3% Nb<sub>2</sub>O<sub>5</sub>/AZ31 (c) 6% Nb<sub>2</sub>O<sub>5</sub>/AZ31

Table 3 Microhardness, Porosity and Density values for Nb<sub>2</sub>O<sub>5</sub>/AZ31 composite

Composition	Micro-hardness	Theoretical density (g/cm <sup>3</sup> )	Actual density (g/cm <sup>3</sup> )	Porosity (%)
AZ31	55.06 ± 7.56	1.77	1.7640	0.3359
3 wt% Nb <sub>2</sub> O <sub>5</sub> /AZ31	58.68 ± 2.85	1.8033	1.7714	1.7710
6 wt% Nb <sub>2</sub> O <sub>5</sub> /AZ31	59.68 ± 5.13	1.8382	1.7684	3.7971

reduction of the lamellar shape ( $\beta$ -Mg<sub>17</sub>Al<sub>12</sub>). This procedure resulted in discontinuity, refining the microstructure for the AZ31 alloy (Abbas and Huang 2020b).

### 3.3 Porosity and density

The porosity and density values of the prepared Nb<sub>2</sub>O<sub>5</sub>/AZ31 composites are shown in Table 3. Differences in porosity and density among the casted composites increased with the weight percentage of the reinforcing particles. As the weight percentage of nano size Nb<sub>2</sub>O<sub>5</sub> increased, the theoretical density value of the composite increased, and the maximum value was obtained at 6 wt% Nb<sub>2</sub>O<sub>5</sub>/AZ31 nanocomposite. The actual densities of the cast composites

were lower than the theoretical density because there are some porosity in the samples. Porosity increased with the weight percentage of the reinforcement increment, and the maximum porosity was found at 6 wt% Nb<sub>2</sub>O<sub>5</sub>/AZ31. In addition to the Nb<sub>2</sub>O<sub>5</sub>, some trapped air in the melt may increase porosity. Also, agglomeration causes the porosity to increase and the actual density of the 6 wt% Nb<sub>2</sub>O<sub>5</sub>/AZ31 to lead decrease. Despite the fact that porosity cannot be completely avoided, it can be managed in the stir casting process. Composites with less than 4% porosity are however acceptable in MMC castings. The actual density and porosity variations in the Nb<sub>2</sub>O<sub>5</sub>/AZ31 nanocomposites may be due to reinforcement particle size, weight fraction of Nb<sub>2</sub>O<sub>5</sub> increases, reduction in wettability, pore nucleation casting deficiencies, and shrinkage during the cooling of casted ingots. Fig. 5(a) indicates changes in porosity and density values of the nanocomposites with different Nb<sub>2</sub>O<sub>5</sub> weight percentages.

### 3.4 Effect of Nb<sub>2</sub>O<sub>5</sub> on the mechanical properties of AZ31

#### 3.4.1 Microhardness

The microhardness of each prepared Nb<sub>2</sub>O<sub>5</sub>/AZ31 nano-

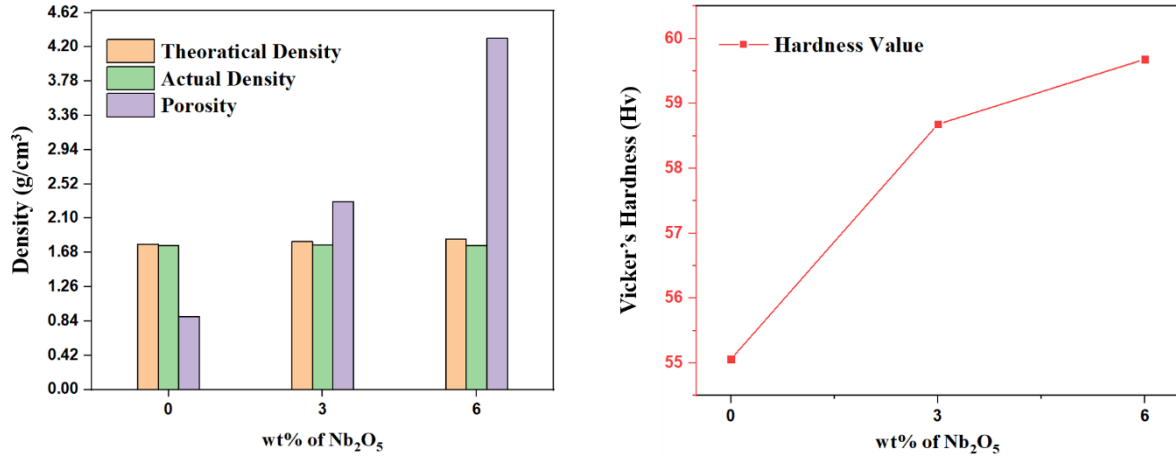


Fig. 5 (a) Density and Porosity and (b) Microhardness values of Nb<sub>2</sub>O<sub>5</sub>/AZ31 nanocomposites

Table 4 Tensile strength comparison of Nb<sub>2</sub>O<sub>5</sub>/AZ31 composites

Sample	Proof Stress (MPa)	UTS (MPa)	Young's Modulus (MPa)	Elongation %
AZ31	80.725 ± 3.70	120.6 ± 8.24	4370.90	5.768 ± 0.3
3 wt% Nb <sub>2</sub> O <sub>5</sub> /AZ31	83.703 ± 2.53	140.4 ± 15.88	4581.19	6.970 ± 4.65
6 wt% Nb <sub>2</sub> O <sub>5</sub> /AZ31	73.912 ± 1.62	126.1 ± 12.22	4184.98	6.932 ± 1.80

composites is presented in Fig. 5(b). Compared with non-reinforced AZ31, the Nb<sub>2</sub>O<sub>5</sub>/AZ31 nanocomposites showed enhancement in microhardness. The hardness of the reinforced composite increased marginally as the volume fraction of the reinforcement particles increased. The microhardness of the nanocomposites containing 3 wt% and 6 wt% Nb<sub>2</sub>O<sub>5</sub>/AZ31 increased by 6.5% and 7.74%, respectively because the  $\beta$ -Mg<sub>17</sub>Al<sub>12</sub> phases in the Mg matrix composites were significantly diffused. Moreover, the uniform distribution of the  $\beta$ -phases and hard reinforcement particles add strength to magnesium alloy by imposing grain refinement contributed positively to increasing the composite's hardness. There is a tendency for particles to agglomeration when the viscosity of the molten metal is higher and there is a higher surface tension between the Nb<sub>2</sub>O<sub>5</sub> and AZ31 alloy melt. Nb<sub>2</sub>O<sub>5</sub>/AZ31 composite's hardness reportedly decreases because of porosity and agglomeration (Huang and Abbas 2020).

### 3.4.2 Tensile Properties

Fig. 6 illustrates the stress-strain curves for the tensile behaviour of the Nb<sub>2</sub>O<sub>5</sub>/AZ31 composites. The AZ31 alloy contained Nb<sub>2</sub>O<sub>5</sub> nanoparticles exhibited an enhancement in yield strength (YS) and ultimate tensile strength (UTS) and elongation as the weight percentages of Nb<sub>2</sub>O<sub>5</sub> increased (Table 4). Therefore, the maximum YS, UTS and elongation of the Nb<sub>2</sub>O<sub>5</sub>/AZ31 were achieved with the addition of 3 wt% Nb<sub>2</sub>O<sub>5</sub>. Furthermore, the addition of 6 wt% Nb<sub>2</sub>O<sub>5</sub> content on AZ31 alloy decreased the YS, UTS and elongation of the Nb<sub>2</sub>O<sub>5</sub>/AZ31 composite. The YS and UTS of the 3 wt% Nb<sub>2</sub>O<sub>5</sub>/AZ31 nanocomposite improved from 80.725 MPa to 83.703 MPa and from 120.6 MPa to 140.4

MPa respectively. Furthermore, increase in the amount of nano Nb<sub>2</sub>O<sub>5</sub> from 3 wt% to 6 wt% resulted in decreases in UTS (from 140.4 MPa to 126.1 MPa) and YS (from 83.703 MPa to 73.912 MPa). The improvements in mechanical properties are related to refinement of the microstructure through dissolution of the  $\beta$  phase. Young's modulus of composites increases with a greater interfacial integrity between the AZ31 alloy and Nb<sub>2</sub>O<sub>5</sub> particulate reinforcement. Nb<sub>2</sub>O<sub>5</sub>/AZ31 nanocomposites have improved tensile properties due to uniform dispersion of Nb<sub>2</sub>O<sub>5</sub> within the matrix and the reinforcing effect generated by it. Tensile strength improved by grain refinement by pinning effect of Nb<sub>2</sub>O<sub>5</sub>, which is consistent with Hall-Petch's mechanism. AZ31 alloy and Nb<sub>2</sub>O<sub>5</sub> have a thermal mismatch, which intensifies dislocations, but the uniform distribution of Nb<sub>2</sub>O<sub>5</sub> prevents movement of dislocations. As a result of the uniform distribution of fine and hard reinforcement, dislocation movement is resulting in increased tensile strength. A reduction in tensile yield strength and UTS occurred because of residual stress created during the deformation or agglomeration of nanoparticles. The drop in UTS was attributed to the clustering of particles and increase in porosity.

The combined effects of reinforced nanoparticles and inhibited growth in grain size after the reduction in dislocation movements greatly increased the hardness and tensile strength. Moreover, the load transfer formed by the inclusion of strengthening phases exerted a substantial effect. The increased hardness, YS and UTS of the casted composites were due to the fundamental strengthening mechanisms of the MMCs, which included the CTE-coefficient of thermal expansion ( $\Delta\alpha_{CTE}$ ), EM-elastic modulus ( $\Delta\alpha_{EM}$ ) among the AZ31 (matrix) and Nb<sub>2</sub>O<sub>5</sub> (reinforcement) strengthening, Orowan strengthening mechanism ( $\Delta\sigma_{OS}$ ) and load transfer effect ( $\Delta\sigma_{LT}$ ) (Huang *et al.* 2021).

The CTEs for AZ31 and Nb<sub>2</sub>O<sub>5</sub> are  $25 \times 10^{-6} K^{-1}$  and  $5.8 \times 10^{-6} K^{-1}$  respectively. CTE values of AZ31 and Nb<sub>2</sub>O<sub>5</sub> varies greatly to contribute the formation of geometrical required dislocations (GNDs) near the grain boundary, resulting in increasing the strength of Nb<sub>2</sub>O<sub>5</sub>/AZ31 composite. The matrix-reinforcement  $\Delta\alpha_{CTE}$  calculated using the Eq. (2) (Rashad *et al.* 2015, Huang *et al.* 2021).

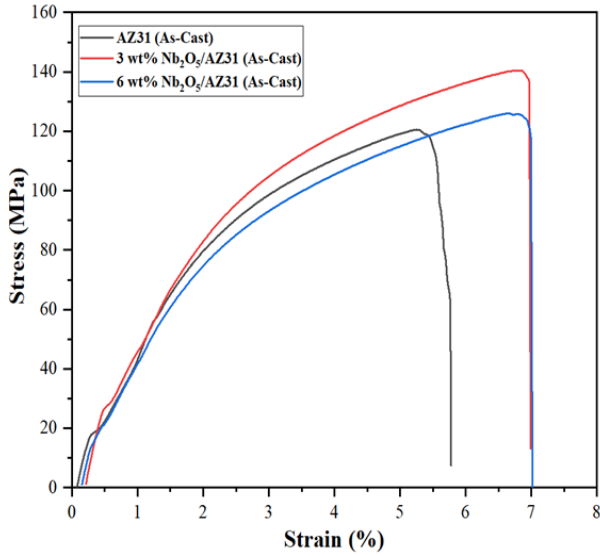


Fig. 6 Stress-Strain curve under Tensile for Nb<sub>2</sub>O<sub>5</sub>/AZ31 Composites

Table 5 Parameters for determining Particle-Induced strengthening contribution

Parameter	Description	Value	Reference/Comment
$\alpha_{Matrix}$	CTE of matrix	$25 \times 10^{-6} K^{-1}$	(Khandelwal <i>et al.</i> 2017)
$\alpha_{Nb_2O_5}$	CTE of Nb <sub>2</sub> O <sub>5</sub>	$5.8 \times 10^{-6} K^{-1}$	(Flaminio <i>et al.</i> 2010)
$\alpha_c$	Difference in CTE of Matrix and Reinforcement	$19.2 \times 10^{-6} K^{-1}$	Calculated Value
$\sigma_{YS}$	YS of matrix (as-cast AZ31)	80.725 MPa	Experimental Value
$b$	Magnitude of Burgers Vector	0.321 nm	(Khandelwal <i>et al.</i> 2017)
$M$	Taylor factor	6.5	(Khandelwal <i>et al.</i> 2017)
$A$	Constant	0.25	(Khandelwal <i>et al.</i> 2017)
$d_h$	Diameter of Nb <sub>2</sub> O <sub>5</sub>	100 nm	Data from manufacturer
$\Delta T$	Processing temperature	300K	Room Temperature
$V_R$	Volume fractions of Nb <sub>2</sub> O <sub>5</sub> particles	0.01176 and 0.02397	Calculated for 3 wt% and 6 wt% Nb <sub>2</sub> O <sub>5</sub> respectively

$$\Delta\alpha_{CTE} = A \times M \times G \times b_{matrix} \times \sqrt{\frac{12\sqrt{2} \times \Delta\alpha_c \times \Delta T \times V_R}{b_{matrix} \times d_h \times (1 - V_R)}} \quad (2)$$

where constant (A), Taylor factor (M), shear modulus (G), burger vector (b), volume fraction ( $V_R$ ) and diameter of the reinforcements ( $d_h$ ). During the heating/cooling fabrication process, the mismatch in coefficient of thermal expansion (CTE) between Nb<sub>2</sub>O<sub>5</sub> and AZ31 alloy contributes to thermal mismatch stress led to heterogeneous interfaces. Dislocations and twins in the matrix are typically responsible for accommodating this stress plastically. The

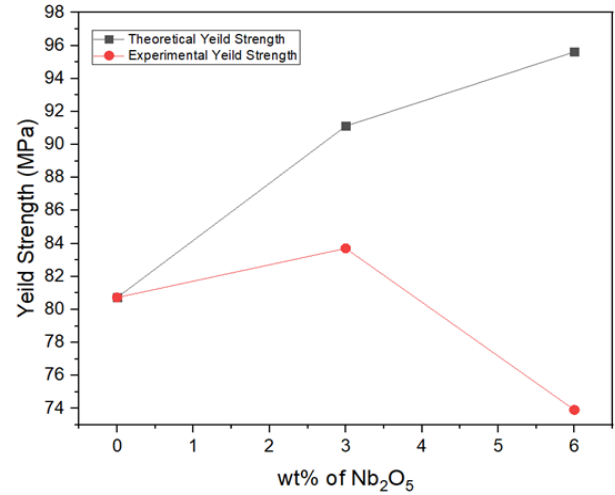


Fig. 7 Comparison of yield Strength of Nb<sub>2</sub>O<sub>5</sub>/AZ31 composites

occurrence of nanoscale twins induced by thermal mismatch stress is more prevalent in composites with smaller particles and higher volume fractions. Dislocations and twins are induced by thermal mismatch stress prior to plastic deformation, resulting in an increase in composite yield strength (Hou *et al.* 2021).

As a result of the EM mismatch between the matrix and reinforcements, the composites have increased strength because significant dislocations are created at their interfaces, as well as geometrical dislocations that are induced at the interface between matrix and reinforcements. The yield strength of the composites vary as a result of the EM mismatch, as the following Eq. (3) (Rashad *et al.* 2015, Huang *et al.* 2021).

$$\Delta\alpha_{EM} = A \times M \times G \times b_{matrix} \times \sqrt{\frac{6 \times V_{HR} \times \varepsilon}{b_{matrix} \times d_{HR}}} \quad (3)$$

where  $\varepsilon$  is elastic strain.

Orowan strengthening is a significant mechanism for nano-sized particle reinforced in metal matrix composites, mainly because of reinforced nanoparticle with small particle sizes and particle spacing can inhibit with the movement of dislocations. The homogeneous distribution of Nb<sub>2</sub>O<sub>5</sub> in the matrix improved YS and the nano reinforced composites have a high strength because of Orowan looping. As a result of these loops, work hardening rates increased. The Orowan strengthening contribution to the yield strength can be expressed by Eq. (4) (Rashad *et al.* 2015, Huang *et al.* 2021).

$$\Delta\sigma_{OS} = \frac{0.4 \times M \times G \times b_{matrix} \times \ln\left(\frac{d_{HR}}{b_{matrix}}\right)}{\pi \times d_{HR} \times \left(\sqrt{\frac{4}{\pi \times V_{HR}}} - 1\right) \times \sqrt{(1 - \nu_{matrix})}} \quad (4)$$

where  $\nu_{matrix}$  is Poisson's ratio.

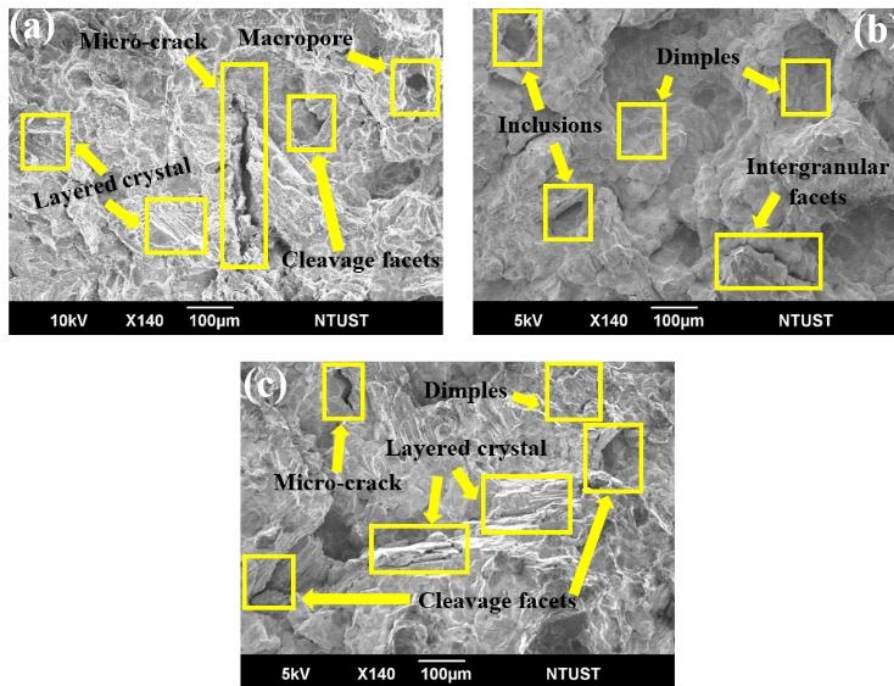
During tensile testing, load transferred from soft matrix to hard nano-reinforcement, especially when the interfacial integrity between the two phases is good and leading to an improvement in composite strength. Because of the small volume fraction of nanoparticles added, the load transfer

Table 6 Contribution of different mechanisms to the weight fraction of nano-Nb<sub>2</sub>O<sub>5</sub>

Sample	$\sigma_p$ (MPa) Experimental	$\sigma_p$ (MPa) Theoretical	$\Delta\alpha_{CTE}$	$\Delta\alpha_{EM}$	$\Delta\sigma_{OS}$	$\Delta\sigma_{LT}$
3 wt% Nb <sub>2</sub> O <sub>5</sub> /AZ31	83.703	91.118	6.436	7.140	3.921	0.475
6 wt% Nb <sub>2</sub> O <sub>5</sub> /AZ31	73.912	95.614	9.246	10.042	5.865	0.968

Table 7 Comparison of mechanical properties

Material	Processing Method	Proof Stress (MPa)	UTS (MPa)	Elongation %	Ref
90.5% AZ31+ 8% SiC	Stir casting	25.21	30.21	7.58	(Sathishkumar <i>et al.</i> 2021)
AZ31D +1% SiC	Stir casting	72.05	114.56	-	(Kumar <i>et al.</i> 2022)
AZ31	Stir casting	80.725 ± 3.70	120.6 ± 8.24	5.768 ± 0.3	
3 wt% Nb <sub>2</sub> O <sub>5</sub> /AZ31	Stir casting	83.703 ± 2.53	140.4 ± 15.88	6.970 ± 4.65	Present Study
6 wt% Nb <sub>2</sub> O <sub>5</sub> /AZ31	Stir casting	73.912 ± 1.62	126.1 ± 12.22	6.932 ± 1.80	

Fig. 8 Fracture surface of (a) AZ31 (b) 3% Nb<sub>2</sub>O<sub>5</sub>/AZ31 (c) 6% Nb<sub>2</sub>O<sub>5</sub>/AZ31

mechanism contributes less. The enhancement of yield strength due to the load transfer is estimated from the following expression Eq. (5) (Rashad *et al.* 2015, Huang *et al.* 2021).

$$\Delta\sigma_{LT} = 0.5 \times V_{HR} \times \sigma_{MYS} \quad (5)$$

where  $\sigma_{MYS}$  - yield strength of cast AZ31 alloy.

A theoretical yield strength ( $\sigma_{CYS}$ ) of the AZ31+ x% Nb<sub>2</sub>O<sub>5</sub> (x=3,6) composites calculated from Eq. (6) and the Table 6 displays the values of different strengthening (Rashad *et al.* 2015, Huang *et al.* 2021)

$$\sigma_{CYS} = \alpha_{MYS} + \sqrt{[(\Delta\alpha_{CTE})^2 + (\Delta\alpha_{EM})^2 + (\Delta\sigma_{OS})^2 + (\Delta\sigma_{LT})^2]} \quad (6)$$

Fig. 7 illustrates the theoretical and experimental YS of the Nb<sub>2</sub>O<sub>5</sub>/AZ31 composites. In order to determine the theoretical yield strength, the ideal materials and assumptions

were considered without defects or imperfections. During fabrication of the composites, there are defects that allow atomic motion, particularly dislocation motion and slip, resulting in shear stresses that made experimental YS of the Nb<sub>2</sub>O<sub>5</sub>/AZ31 composites lower than those predicted theoretically. The tensile strengths of the composites were reduced when high amounts of Nb<sub>2</sub>O<sub>5</sub> (6 wt%) particles were added due to the residual stress was produced through agglomeration or deformation.

### 3.4.3 Fractography

Fig. 8(a) shows the fractographic surface morphology of pure AZ31 and AZ31 reinforced using 3% and 6% of Nb<sub>2</sub>O<sub>5</sub>. As usual the pure AZ31 magnesium alloy showed a high intensity of brittleness which can be justified by the fracture surface image analysis. With a variety of fracture mechanics like cleavage facets, layered crystals, micro-

cracks, and macropores. The micro-crack grown from the cleavage facets seems an issue in pure AZ31. The micro-crack being transgranular in the as-cast pure AZ31 makes it noticeable that most of the fracture categories belong to brittle fractures. Hence the as-cast AZ31 might show less strength compared to reinforced Nb<sub>2</sub>O<sub>5</sub>/AZ31. Fig. 8(b) features the change in fracture mechanics with the addition of reinforcement 3% Nb<sub>2</sub>O<sub>5</sub>/AZ31. The increase in dimple number and diameter shows a direct improvement in elongation percentage by approximately 28.8% then as-cast. With the addition of Nb<sub>2</sub>O<sub>5</sub>, the XRD result shows a small intensity of the new  $\beta$ -phase i.e., Mg(Nb<sub>2</sub>O<sub>6</sub>) with Mg<sub>12</sub>Al<sub>7</sub> which was found in pure AZ31. The inclusion found in the fracture morphology of 3% Nb<sub>2</sub>O<sub>5</sub>/AZ31 might be because of the oxygen in Mg(Nb<sub>2</sub>O<sub>6</sub>). But the image analysis shows a reduction in major crack formation. The increase in dimples and the reduction of cleavage and layered crystal imply that the failure is mostly ductile in nature. Fig. 8(c) shows the mixed mode of fracture consists of dimples, cleavages, layered crystal, and micro-crack. The general grouping of fracture types can be done i.e., cleavage, and layered crystals are the proof of brittle fracture. The increase in reinforcement percentage might create a precipitation localization around the grain boundary, and the cleavage facets initiated the crack tip and the local inhomogeneity induced the local stress around the grain boundary and the crack being followed through the boundary. But the dimples can also be seen in the morphology providing evidence of ductile fracture. The elongation value shows a reduction compared to 3% Nb<sub>2</sub>O<sub>5</sub>/AZ31. In the mixed mode of fracture, it can be concluded that the dominance is brittle cracks.

According to the determined results of the Nb<sub>2</sub>O<sub>5</sub>/AZ31 composites, the microhardness, yield strength and elongation have significant increase in the Nb<sub>2</sub>O<sub>5</sub>/AZ31 composites compared to as cast AZ31 alloy. Upon increasing the composition of Nb<sub>2</sub>O<sub>5</sub> to 3 wt% in the composites, mechanical properties began to increase and subsequently decreased as volume proportions increased to 6 wt %, respectively.

#### 4. Conclusions

The stir casting method was successfully used in fabricating AZ31/Nb<sub>2</sub>O<sub>5</sub> nanocomposites. The effects of nano size Nb<sub>2</sub>O<sub>5</sub> on microstructure and mechanical properties were investigated. As a result of the analysis, the following major conclusions were reached:

- Owing to the presence of Nb<sub>2</sub>O<sub>5</sub> particles in the composite, significant grain refinement was achieved. As the Mg<sub>17</sub>Al<sub>12</sub> phases exerted effects that inhibited improvement in mechanical properties, Nb<sub>2</sub>O<sub>5</sub> addition dissolved the precipitates and reduced their thickness, resulting in discontinuity and refined microstructure for the AZ31 alloy.

- The tensile strength was improved by reinforcing the Nb<sub>2</sub>O<sub>5</sub> nanoparticles with matrix AZ31 alloy. However, the 3 wt% Nb<sub>2</sub>O<sub>5</sub>/AZ31 composite had a maximum tensile strength of 140.4 MPa. As concentrations of Nb<sub>2</sub>O<sub>5</sub> increased, the strengthening contribution that the particles

provide also increased.

- The nano-Nb<sub>2</sub>O<sub>5</sub> particles contributed significantly to the strengthening of the matrix, and strengthening contribution increased with nano-Nb<sub>2</sub>O<sub>5</sub> particle concentration. EM contributed more significantly to strengthening than the Orowan mechanism regardless of Nb<sub>2</sub>O<sub>5</sub> nanoparticle fraction and volume fraction.

#### Acknowledgments

The authors would like to thank the Ministry of Science and Technology, Taiwan (MOST 109-2224-E-011-002-) for providing financial support.

#### References

- Abbas, A. and Huang, S.J. (2020a), "Qualitative and quantitative investigation of As-Cast and aged CNT/AZ31 metal matrix composites," *J. Miner. Metals Mater. Soc.*, **72**(6), 2272-2282. <https://doi.org/10.1007/s11837-020-04114-7>.
- Abbas, A. and Huang, S.J. (2020b), "Investigation of severe plastic deformation effects on microstructure and mechanical properties of WS<sub>2</sub>/AZ91 magnesium metal matrix composites," *Mater. Sci. Eng. A*, **780**(January), 139211. <https://doi.org/10.1016/j.msea.2020.139211>.
- Abbas, A. and Huang, S.J. (2021), "Investigating the hall-petch constants for as-cast and aged az61/cnts metal matrix composites and their role on superposition law exponent," *J. Compos. Sci.*, **5**(4). <https://doi.org/10.3390/jcs5040103>.
- Alaneme, K.K., Adu, O.P., Oke, S.R., Falodun, O.E. and Olubambi, P.A. (2020a), "Densification characteristics, microstructure and wear behaviour of spark plasma sintering processed titanium-niobium pentoxide (Ti-Nb<sub>2</sub>O<sub>5</sub>) based composites", *J. King Saud Univ. Eng. Sci.*, <https://doi.org/10.1016/j.jksues.2020.10.005>.
- Alaneme, K.K., Fatokun, A.A., Oke, S.R. and Olubambi, P.A. (2020b), "Nanoindentation studies and analysis of the mechanical properties of Ti-Nb<sub>2</sub>O<sub>5</sub> based composites", *Manuf. Rev.*, **7**. <https://doi.org/10.1051/mfreview/2020017>.
- Ali Ghorbanpour Arani, A.F. and M.M. (2021), "The effect of nanoparticles on enhancement of the specific mechanical properties of the composite structures: A review research", *Adv. Nano Res.*, **10**(4), 327-337. <https://doi.org/https://doi.org/10.12989/anr.2021.10.4.327>.
- Bains, P.S., Sidhu, S.S. and Payal, H.S. (2016), "Fabrication and machining of metal matrix composites: A review", *Mater. Manuf. Proc.*, **31**(5), 553-573. <https://doi.org/10.1080/10426914.2015.1025976>.
- Banerjee, S., Poria, S., Sutradhar, G. and Sahoo, P. (2019), "Dry sliding tribological behavior of AZ31-WC nano-composites", *J. Magnesium Alloys*, **7**(2), 315-327. <https://doi.org/10.1016/j.jma.2018.11.005>.
- Borodianskiy, K. and Zinigrad, M. (2015), "mechanical properties and microstructure characterization of Al-Si cast alloys formation using carbide nanoparticles", *J. Mater. Sci. Appl.*, **1**(3), 85-90.
- Chen, L.Y., Xu, J.Q., Choi, H., Pozuelo, M., Ma, X., Bhowmick, S., et al. (2015), "Processing and properties of magnesium containing a dense uniform dispersion of nanoparticles", *Nature*, **528**(7583), 539-543. <https://doi.org/10.1038/nature16445>.
- Da Silva, A.L., Hotza, D. and Castro, R.H.R. (2017), "Surface energy effects on the stability of anatase and rutile nanocrystals: A predictive diagram for Nb<sub>2</sub>O<sub>5</sub>-doped-TiO<sub>2</sub>", *Appl. Surf. Sci.*,

- 393**, 103-109. <https://doi.org/10.1016/j.apsusc.2016.09.126>.
- Dey, A. and Pandey, K.M. (2015), "Magnesium metal matrix composites-a review", *Rev. Adv. Mater. Sci.*, **42**(1), 58-67.
- Dinakaran, I., Vettivel, S.C., Balakrishnan, M. and Akinlabi, E.T. (2019), "Influence of processing route on microstructure and wear resistance of fly ash reinforced AZ31 magnesium matrix composites", *J. Magnesium Alloys*, **7**(1), 155-165. <https://doi.org/10.1016/j.jma.2019.01.003>.
- Dinakaran, I., Zhang, S., Chen, G. and Shi, Q. (2020), "Titanium particulate reinforced AZ31 magnesium matrix composites with improved ductility prepared using friction stir processing", *Mater. Sci. Eng. A*, **772**, 138793. <https://doi.org/10.1016/j.msea.2019.138793>.
- Flaminio, R., Franc, J., Michel, C., Morgado, N., Pinard, L. and Sassolas, B. (2010), "A study of coating mechanical and optical losses in view of reducing mirror thermal noise in gravitational wave detectors", *Classical Quantum Gravity*, **27**(8). <https://doi.org/10.1088/0264-9381/27/8/084030>.
- Hassan, S.F. and Gupta, M. (2006), "Effect of type of primary processing on the microstructure, CTE and mechanical properties of magnesium/alumina nanocomposites", *Compos. Struct.*, **72**(1), 19-26. <https://doi.org/10.1016/j.compstruct.2004.10.008>.
- Hou, Y. N., Yang, K. M., Song, J., Wang, H., Liu, Y. and Fan, T. X. (2021), "A crystal plasticity model for metal matrix composites considering thermal mismatch stress induced dislocations and twins", *Sci. Rep.*, **11**(1), 1-13. <https://doi.org/10.1038/s41598-021-95439-z>.
- Huang, S.J., Subramani, M. and Chiang, C.C. (2021), "Effect of hybrid reinforcement on microstructure and mechanical properties of AZ61 magnesium alloy processed by stir casting method", *Compos. Commun.*, **25**, 100772. <https://doi.org/10.1016/j.coco.2021.100772>.
- Huang, S.J. and Abbas, A. (2020), "Effects of tungsten disulfide on microstructure and mechanical properties of AZ91 magnesium alloy manufactured by stir casting", *J. Alloys Compd.*, **817**, 153321. <https://doi.org/10.1016/j.jallcom.2019.153321>.
- Huang, S.J. and Ali, A.N. (2018), "Effects of heat treatment on the microstructure and microplastic deformation behavior of SiC particles reinforced AZ61 magnesium metal matrix composite", *Mater. Sci. Eng. A*, **711**, 670-682. <https://doi.org/10.1016/j.msea.2017.11.020>.
- Idrisi, A.H. and Mourad, A.H.I. (2019), "Conventional stir casting versus ultrasonic assisted stir casting process: Mechanical and physical characteristics of AMCs", *J. Alloys Compd.*, **805**, 502-508. <https://doi.org/10.1016/j.jallcom.2019.07.076>.
- Khandelwal, A., Mani, K., Srivastava, N., Gupta, R. and Chaudhari, G.P. (2017), "Mechanical behavior of AZ31/Al<sub>2</sub>O<sub>3</sub> magnesium alloy nanocomposites prepared using ultrasound assisted stir casting", *Compos. Part B Eng.*, **123**, 64-73. <https://doi.org/10.1016/j.compositesb.2017.05.007>.
- Kumar, K.C.K., Kumar, B.R. and Rao, N.M. (2022), "Microstructural, mechanical characterization, and fractography of AZ31/SiC reinforced composites by stir casting method", *Silicon*, **14**(9), 5017-5027. <https://doi.org/10.1007/s12633-021-01180-7>.
- Ma, G., Xiao, H., Ye, J. and He, Y. (2020), "Research status and development of magnesium matrix composites", *Mater. Sci. Technol.*, **0**(0), 1-9. <https://doi.org/10.1080/02670836.2020.1732610>.
- Malaki, M., Tehrani, A.F., Niroumand, B. and Gupta, M. (2021), "Wettability in metal matrix composites", *Metals*, **11**(7), 1-24. <https://doi.org/10.3390/met11071034>.
- Rahman, M.W. (2019), "Preparation of magnesium diniobate by solid-state reactions and its role for hydrogen storage", *J. Australian Ceram. Soc.*, **55**(2), 579-586. <https://doi.org/10.1007/s41779-018-0265-5>.
- Rashad, M., Pan, F., Guo, W., Lin, H., Asif, M. and Irfan, M. (2015), "Effect of alumina and silicon carbide hybrid reinforcements on tensile, compressive and microhardness behavior of Mg-3Al-1Zn alloy", *Mater. Character.*, **106**, 382-389. <https://doi.org/10.1016/j.matchar.2015.06.033>.
- Safavi, M. S., Walsh, F. C., Visai, L. and Khalil-Allafi, J. (2022), "Progress in niobium oxide-containing coatings for biomedical applications: A critical review", *ACS Omega*, **7**(11), 9088-9107. <https://doi.org/10.1021/acsomega.2c00440>.
- Sameer Kumar, D., Suman, K.N.S., Tara Sasanka, C., Ravindra, K., Poddar, P. and Venkata Siva, S.B. (2017), "Microstructure, mechanical response and fractography of AZ91E/Al<sub>2</sub>O<sub>3</sub> (p) nano composite fabricated by semi solid stir casting method", *J. Magnesium Alloys*, **5**(1), 48-55. <https://doi.org/10.1016/j.jma.2016.11.006>.
- Sathishkumar, P., Deepakaravind, V., Gopal, P. and Azhagiri, P. (2021), "Analysis the mechanical properties and material characterization on Magnesium Metal Matrix Nano composites through stir casting process", *Mater. Today Proceedings*, **46**, 7436-7441. <https://doi.org/10.1016/j.matpr.2021.01.041>.
- Selivorstov, V., Dotsenko, Y. and Borodianskiy, K. (2017), "Influence of low-frequency vibration and modification on solidification and mechanical properties of Al-Si casting alloy", *Materials*, **10**(5). <https://doi.org/10.3390/ma10050560>.
- Shen, M.J., Zhang, M.F. and Jia, J.H. (2020), "Deformation behavior and microstructure evolution of AZ31B composites containing multiscale distribution during room temperature tensile", *J. Alloys Compd.*, **820**, 153446. <https://doi.org/10.1016/j.jallcom.2019.153446>.
- Silva, C., Montoro, L.A., Martins, D.A.A., Machado, P.A., Pereira, P.H.R., Gonzalez, B.M., et al. (2020), "Interface structures in Al-Nb<sub>2</sub>O<sub>5</sub> nanocomposites processed by high-pressure torsion at room temperature", *Materials Characterization*, **162**, 110222. <https://doi.org/10.1016/j.matchar.2020.110222>.
- Vini, M. H. and Daneshmand, S. (2020), "Effect of TiO<sub>2</sub> particles on the mechanical and microstructural evolution of hybrid aluminum-based composites fabricated by Warb", *Surf. Rev. Lett.*, **27**(12), 99-107. <https://doi.org/10.1142/S0218625X20500262>.
- Zhao, K.N., Li, H.X., Luo, J.R., Liu, Y.J., Du, Q. and Zhang, J.S. (2017), "Interfacial bonding mechanism and mechanical properties of novel AZ31/WE43 bimetal composites fabricated by insert molding method", *J. Alloys Compd.*, **729**, 344-353. <https://doi.org/10.1016/j.jallcom.2017.09.166>.
- Zhou, M.Y., Ren, L.B., Fan, L.L., Zhang, Y.W.X., Lu, T.H., Quan, G.F., et al. (2020), "Progress in research on hybrid metal matrix composites", *J. Alloys Compd.*, **838**. <https://doi.org/10.1016/j.jallcom.2020.155274>.
- Zhu, J., Yang, W., Yang, H. and Wang, F. (2011), "Effect of Nb<sub>2</sub>O<sub>5</sub> on the microstructure and mechanical properties of TiAl based composites produced by hot pressing", *Mater. Sci. Eng. A*, **528**(21), 6642-6646. <https://doi.org/10.1016/j.msea.2011.04.062>.